Solution Structure of the Apo and Copper(I)-Loaded Human Metallochaperone HAH1[†]

Ioanna Anastassopoulou,[‡] Lucia Banci,[§] Ivano Bertini,*[,§] Francesca Cantini,[§] Efthalia Katsari,[§] and Antonio Rosato[§]

Institute of Physical Chemistry, NCSR "Demokritos", 153 10 Aghia Paraskevi Attikis, Greece, and Magnetic Resonance Center (CERM), University of Florence, Via Luigi Sacconi 6, 50019 Sesto Fiorentino, Italy

Received June 15, 2004; Revised Manuscript Received July 31, 2004

ABSTRACT: The human metallochaperone HAH1 has been produced in *Escherichia coli* with four additional amino acids at the C-terminus and characterized in solution by NMR spectroscopy, both with and without copper(I). The solution structure of the apo-HAH1 monomer has a root-mean-square-deviation (RMSD) of 0.50 Å for the coordinates of the backbone atoms and 0.96 Å for all heavy atoms. These values compare, respectively, with 0.45 and 0.95 Å for copper(I)−HAH1. There are only minor structural rearrangements upon copper(I) binding. In particular, the variation of interatomic interactions around the metal-binding region is limited to a movement of Lys60 toward the metal site. The protein structures are similar to those obtained by X-ray crystallography in a variety of derivatives, with backbone RMSD values below 1 Å. In the holoprotein, copper(I) is confirmed to be two coordinated. If these data are compared with those of orthologue proteins, we learn that HAH1 has a lower tendency to change coordination number from two to three. Such a switch in coordination is a key step in copper transfer.

Copper, an essential trace metal, is utilized as a cofactor in a variety of proteins. Excess copper, however, is highly toxic to most organisms (*1*, *2*). Accordingly, a complex machinery of proteins that bind the metal ion strictly controls the uptake, transport, sequestration, and efflux of copper in vivo (*3*−*5*). In particular, so-called metallochaperones deliver copper to specific intracellular targets, acting like enzymes to lower the activation barrier for copper transfer to their specific partners (*6*), thereby circumventing the significant thermodynamic overcapacity for copper chelation of the cytoplasm (*7*). Several structural studies have addressed at the atomic level the coordination of copper and the mechanisms for copper transfer between partners in different biological pathways (*8*, *9*).

One of the human copper chaperones is HAH1 (also called human Atx1 or Atox1), a small soluble protein (*10*, *11*) which is capable of delivering copper(I) both to the Menkes and the Wilson disease proteins (ATP7A and ATP7B, respectively) (*3*−*5*). The latter two proteins are membrane-bound P-type ATPases which translocate copper in the trans-Golgi network or across the plasma membrane (*3*−*5*), depending on the environmental conditions (*12*). Both ATP7A and ATP7B possess six copper(I)-binding domains, which are similar in sequence to HAH1. Homologues of both HAH1 and ATP7A/ATP7B are found in a number of prokaryotic and eukaryotic organisms; however, it is noteworthy that the genome of some organisms may encode only one of the two partners (*13*).

Copper transfer from HAH1 to its physiological partners is indeed the subject of intense very recent experimental work. Intriguing results have been obtained on the kinetics of copper loading in the six binding domains of ATP7B, where the second binding domain has been shown to act as the first entry point of copper(I) upon delivery by HAH1 (*14*). The structure of the corresponding domain of ATP7A is available (*15*, *16*). On the other hand, the affinity equilibrium constants for the binding of HAH1 for the six ATP7A soluble domains are very similar to each other, as judged by surface plasmon resonance (*17*). It is also interesting to note that copper(I) uptake confers to the metal-binding cysteines in the six ATP7B domains different protection toward chemical modification, depending on whether the metal is received from HAH1 or from a copper(I) solution (*14*). This indicates that protein−protein interaction is responsible for directing copper transfer as a result of kinetic control of the transfer reaction (*14*).

The affinities for copper(I) of HAH1 and of the ATP7B domains have been determined recently by isothermal titration calorimetry (ITC) (*18*). It appears that the chaperone and the partner domains have similar binding constants, with HAH1 being at the lower end of the range spanned. The data for ATP7B constructs containing a different number of copper-binding domains suggest that conformational rearrangements take place upon copper binding, or at least play a role in tuning the affinity of ATP7B for copper. Given also the significant variability of electrostatic surface properties among the six ATP7B domains, it has been suggested that in addition to HAH1−ATP7B interactions also inter-domain interactions with the various domains of ATP7B are important for copper transport (*18*).

[†] This work was supported by MIUR-COFIN 2003, by Ente Cassa di Risparmio di Firenze (PROMELAB project), by the European Commission (Contract No. QLG2-CT-2002-00988), and by the European Community (SPINE No. QLG2-CT-2002-00988, "Structural proteomics in Europe").

* To whom correspondence should be addressed. Fax: +39 055 4574271. Phone: +39 055 4574272. E-mail: bertini@cerm.unifi.it.

[‡] NCSR "Demokritos".

[§] University of Florence.

10.1021/bi0487591 CCC: $27.50 © 2004 American Chemical Society
Published on Web 09/25/2004

The work on the yeast homologues of human HAH1 and ATP7A/ATP7B (Atx1 and Ccc2, respectively) has provided a wealth of intriguing atomic-level details on copper transfer between the metallochaperone and its partner ATPase (*19*, *20*). However, as briefly outlined above, the human systems show a significantly higher level of complexity, which is likely to be very relevant for the understanding of the determinants of the Menkes and Wilson diseases. The X-ray structure of HAH1 is available, in complex with different metal ions: copper(I), cadmium(II), mercury(II) (*21*). In all these structures, the metal ion is coordinated by three or four cysteines from the metal-binding sites of two protein molecules, so that the metal:protein stoichiometry is always 1:2 (*21*). In the present work we present a detailed structural and dynamic characterization of the behavior of human HAH1 in solution, in the two physiologically relevant forms (reduced apo and copper(I)-bound). Some distinct differences with respect to yeast Atx1 are observed.

MATERIALS AND METHODS

Protein Expression and Purification. The DNA sequence encoding HAH1 was amplified via PCR from human cDNA and cloned into pET20b+ (Novagen) between the *Nde*I and *Xho*I restriction sites, so that the expressed protein additionally contains a recognition site for the restriction protease Factor Xa and $(His)_6$ tag at the C-terminal end. After cleavage of the tag, four amino acids from the restriction site are left at the C-terminus of the protein.

The above-described plasmid was transformed into *Escherichia coli* strain BL21(DE3)Gold for protein expression. Cells were grown at 37 °C in M9 minimal media containing $(NH_4)_2SO_4$ as the sole nitrogen source and glucose as the sole carbon source. The medium was supplemented with a vitamin mix and a trace metal solution. Ampicillin (100 μg/mL) was added to the culture medium. Stable isotope-enriched samples were produced using >95% enriched nitrogen and carbon sources, as appropriate. Protein expression was induced using 1 mM isopropyl 1-thio-β-D-galactopyranoside when A_{600} was ~0.6, and the cells were harvested 4 h thereafter. The typical protein yield was 30−40 mg of pure protein/L of culture.

All protein purification steps were carried out in a N_2 atmosphere chamber by affinity chromatography with a HiTrap 5 mL affinity column (Amersham Pharmacia Biotech) previously charged with Zn^{2+}. After purification, the $(His)_6$ tag could be cut by overnight incubation with Factor Xa (40 μg of enzyme/20 mg of recombinant protein). The protein without the $(His)_6$ tag was purified by passing the solution again through the HiTrap column charged with Zn^{2+}, under conditions where the uncut protein would stick to the column.

The recombinant protein finally produced was characterized by mass spectroscopy (ESI-MS, under nondenaturing conditions) and copper atomic absorption. Colorimetric determinations using the copper(I) ligand bathocuproine disulfonate (BCS) were employed to assess the relative copper content in different samples.

NMR Sample Preparation. Apoprotein samples were reduced with excess dithiothreitol (DTT) and washed with 100 mM sodium phosphate buffer at pH 7.0. The final molar ratio of DTT to protein was typically 2−5-fold.

Copper(I)-containing protein samples were prepared following two different approaches. In one approach DTT was added to a dilute (0.1−0.5 mM) protein solution in 100 mM sodium phosphate buffer at pH 7.0 with a 10-fold DTT:protein ratio, followed by a 2−3-fold excess of $CuSO_4$. The protein was then concentrated and washed with buffer containing 2−4 mM DTT as appropriate to achieve a 2-fold DTT:protein ratio in the final NMR sample. In the second approach, a dilute protein solution in 10 mM sodium acetate at pH 6.0 was reduced with a 5-fold excess of DTT, and copper was then added using a small excess of the copper(I) complex $[Cu(CH_3CN)_4]^+$. The protein was then concentrated and washed with the acetate buffer containing no DTT.

The final protein concentration in all samples was between 1 and 2 mM. NMR samples also contained 10% v/v ^2H_2O for NMR spectrometer lock.

NMR Spectra and Structural Calculations. All 2D and 3D spectra were collected at 298 K, unless otherwise indicated, processed using the standard Bruker software (XWINNMR), and analyzed using the XEASY program (*22*). Tables S1 and S2 in the Supporting Information summarize the experiments performed on apo-HAH1 and copper(I)−HAH1, respectively.

The peaks used for structure calculations were integrated in the 2D NOESY[1] map, as well as in the 3D ^{15}N and ^{13}C NOESY−HSQC spectra. Intensities of dipolar connectivities were converted into upper distance limits using the program CALIBA (*23*). Each peak list was calibrated independently.

$^3J_{HN-H\alpha}$ coupling constants were used to derive constraints for the backbone dihedral angle ϕ by means of the appropriate Karplus curve (*24*). ϕ angle constraints were further obtained from the ratio between intraresidue and sequential HN−Hα NOESY cross-peak intensities (*25*) and the secondary structure indicated by the chemical shift index (CSI) (*26*), both of which were used also to extract ψ torsion angles.

Structure Calculations. Structure calculations were performed using the program CYANA (*27*). The CANDID module of CYANA (*28*) was exploited for automated assignment of the NOESY cross-peaks, followed by a manual check prior to the final calculations. A total of 400 random conformers were annealed in 8000 steps using the above constraints. The 30 conformers with the lowest target function constituted the final family.

The copper ion was included in the calculations following a procedure already reported, which does not impose any fixed orientation of the ligands with respect to the copper (*29*). Restrained energy minimization (REM) was performed for each member of the final family of conformers using the AMBER 6 package (*30*). The force field parameters for the copper(I) ion were taken as in similar systems (*31*). Force constants of 32 kcal mol^{-1} Å^{-2} and 50 kcal mol^{-1} rad^{-2} were used for NOE and torsion angle constraints, respectively.

The quality of the structure was evaluated in terms of deviations from ideal bond lengths and bond angles and through Ramachandran plots obtained using the programs

[1] Abbreviations: RMSD, root-mean-square deviation; TOCSY, total correlation spectroscopy; NOE, nuclear Overhauser effect; NOESY, nuclear Overhauser effect spectroscopy; HMQC, heteronuclear multiple quantum coherence; HSQC, heteronuclear single-quantum coherence; INEPT, insensitive nuclei enhanced by polarization transfer; DTT, dithiothreitol.

PROCHECK (*32*) and PROCHECK-NMR (*33*). Structure calculations and analysis were performed on a cluster of Linux PCs.

NMR Mobility Data Acquisition and Analysis. NMR experiments for determination of ^{15}N longitudinal and traversal relaxation rates (*34*) and ^{1}H−^{15}N NOE values (*35*) were recorded at 298 K at 600 MHz. R_1 and R_2 relaxation rates were obtained by fitting the cross-peak volumes (*I*), measured as a function of the relaxation delay, to a single-exponential decay by using the Levenberg−Marquardt algorithm (*36*), as described in the literature (*37*). Uncertainties had been evaluated by using a Monte Carlo approach (*37*). Heteronuclear NOE values were calculated as the ratio of peak volumes in spectra recorded with and without saturation.

RESULTS

Protein Characterization. Mass spectroscopy confirmed the expected weight for the present HAH1 construct, including the extra four amino acids at the protein C-terminus, which are left after cleavage of the protein with the protease factor Xa. Copper atomic absorption data for protein samples prepared by using an acetonitrile complex to deliver copper(I) to HAH1 indicate binding of a single metal ion per protein molecule.

Apo-HAH1 and copper(I)−HAH1 samples were found to be quite soluble and are stable at millimolar concentration for weeks. Both apo-HAH1 and copper(I)−HAH1 show well-resolved and well-dispersed ^{1}H−^{15}N HSQC spectra, indicative of folded proteins.

NMR Spectral Assignment and Structural Calculations. Backbone assignments were obtained using standard strategies based on triple-resonance experiments (*38*). A total of 64 out of the expected 65 ^{15}N backbone amide resonances were assigned. The amide group of residue Gly13 could not be detected in both apo-HAH1 and copper(I)−HAH1.

The assignment of the side chain resonances was performed through the analysis of the 3D (H)CCH TOCSY spectrum together with ^{15}N NOESY−HSQC and ^{13}C NOESY−HSQC spectra. The assignment of the aromatic spin systems was performed with 2D NOESY and TOCSY maps. In this way more than 90% of the total ^{1}H, ^{15}N, and ^{13}C resonances were assigned. The resonance assignments, for apo-HAH1 and copper(I)−HAH1, are reported as Supporting Information (Tables S3 and S4). The combined variation (*39*) of the ^{15}N and HN chemical shifts between apo-HAH1 and copper(I)−HAH1 is shown in Figure 1. It appears that all major chemical shift variations occurring consistently for the two nuclei are located between residue 10 and residue 18, i.e., from two residues before the first copper(I) ligand (Cys12) up to three residues after the second copper(I) ligand (Cys15).

Solution Structures. Totals of 1284 and 1383 meaningful structural constraints were used for structure calculations of apo-HAH1 and copper(I)−HAH1, respectively. A breakdown of the constraints used is given in Tables 1 and 2 for apo-HAH1 and copper(I)−HAH1, respectively. The NOE constraints used for all calculations are listed in the Supporting Information (Tables S5 and S6).

The final (after REM refinement) apo-HAH1 family has an average total target function of 0.20 ± 0.02 Å^2, while the corresponding value for the copper(I)−HAH1 family is 0.18 ± 0.02 Å^2. The average backbone RMSD values (over residues 2−68) for the apo-HAH1 and copper(I)−HAH1 structures are, respectively, 0.52 ± 0.06 and 0.45 ± 0.09 Å; the all heavy atom RMSD values instead are, respectively, 0.97 ± 0.10 and 0.94 ± 0.11 Å. Tables 1 and 2 report some statistics on constraint violations in the final families together with selected quality parameters from a PROCHECK-NMR (*33*) analysis. These data indicate that the solution structures obtained for both apo-HAH1 and copper(I)−HAH1 are of good quality.

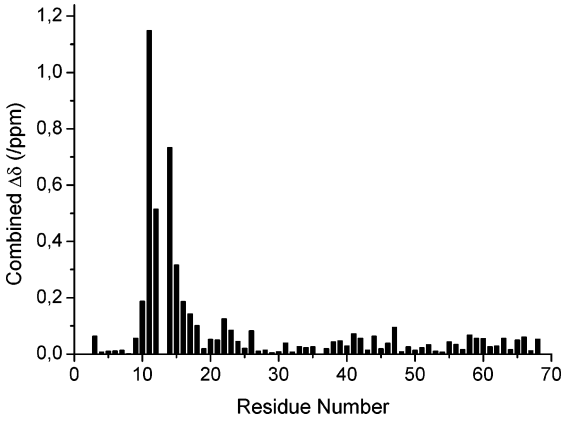

FIGURE 1: Combined chemical shift variation ($\Delta\delta$) for backbone ^{15}N and HN nuclei between apo-HAH1 and copper(I)−HAH1. $\Delta\delta$ values have been calculated using the equation given in ref *39*.

Figure 2A,B shows a comparison of the structures of apo-HAH1 and copper(I)−HAH1, highlighting the metal site structure in the latter. Both structures adopt the ferredoxin-like $\beta\alpha\beta\beta\alpha\beta$ fold, as also found in the solid state (*21*, *40*) (Figure 2). The RMSD between the backbone atoms for the mean structures of the two families of conformers, excluding the metal-binding loop region and the poorly defined terminal tails, is below 1.0 Å. Table 3 shows the elements of secondary structure detected by PROCHECK-NMR in the two structures.

The sulfur−copper−sulfur angle in copper(I)−HAH1 is found to be 160° ± 25°. This value is consistent with the linear digonal coordination observed by EXAFS (*41*).

Protein Dynamics in Solution. Apo-HAH1 exposed to air in the absence of DTT in solution was found to dimerize readily, as observed by SDS−PAGE gels and by the line width observed in ^{1}H−^{15}N HSQC experiments (not shown). Samples prepared in an anaerobic chamber and containing a 2-fold excess of DTT were instead found to be monomeric, as indicated by a mean ^{15}N R_1 value (at 14 T) of 2.7 ± 0.4 s^{-1} and a mean R_2 value of 6.2 ± 0.8 s^{-1}. Per-residue ^{15}N R_1 and R_2 values are shown in Figure 3. Similarly, different copper(I)−HAH1 preparations could yield either dimeric or monomeric protein, having the same 1:1 copper(I):protein ratio. Dimers and monomers could be readily distinguished by ^{15}N R_1 and R_2 values. The mean ^{15}N R_1 value (at 14 T) for monomeric copper(I)−HAH1 is 2.4 ± 0.2 s^{-1}, and the mean R_2 value is 6.8 ± 1.3 s^{-1}. Some residual line broadening is present for residues 11−14, probably due to conformational averaging (Figure 3).

The observed ^{15}N R_1 and R_2 values together with ^{1}H−^{15}N NOE values (not shown) indicated that, in both the apo- and

Table 1: Statistical Analysis of the Energy-Minimized Family of Conformers and the Mean Structure of Apo-HAH1

	REM[a] (30 structures)	⟨REM⟩[a] (mean)
RMS violations per meaningful distance constraint (Å)[b]		
intraresidue (266)	0.0026 ± 0.0027	0.0209
sequential (310)	0.0142 ± 0.0017	0.0140
medium-range (241)[c]	0.0113 ± 0.0024	0.0145
long-range (369)	0.0095 ± 0.0013	0.0089
total (1186)	0.0160 ± 0.0011	0.0147
RMS violations per meaningful dihedral angle constraint (deg)[b]		
ϕ (49)	1.13 ± 0.66	1.32
ψ (49)	0.82 ± 0.19	0.96
average number of constraints per residue	17	
average number of violations per structure		
intraresidue	14.3 ± 2.5	11
sequential	7.8 ± 1.8	10
medium-range	4.7 ± 1.6	8
long-range	5.4 ± 1.1	5
total	32.0 ± 4.4	34
ϕ	2.3 ± 0.8	3
ψ	1.5 ± 0.6	3
average number of NOE violations larger than 0.3 Å	0.0 ± 0.0	0.00
average number of NOE violations between 0.1 and 0.3 Å	8.8 ± 2.3	5.00
structural analysis[d]		
% of residues in most favorable regions	86.2	86.2
% of residues in allowed regions	13.6	13.8
% of residues in generously allowed regions	0.2	0.0
% of residues in disallowed regions	0.0	0.0
experimental restraints analysis[e]		
% completeness of experimentally observed NOEs up to a 4 Å cutoff distance	62	58
% completeness of experimentally observed NOEs up to a 5 Å cutoff distance	44	39

[a] REM indicates the energy-minimized family of 30 structures, and ⟨REM⟩ is the energy-minimized mean structure obtained from the coordinates of the individual REM structures. [b] The number of meaningful constraints for each class is reported in parentheses. [c] Medium-range distance constraints are those between residues i and $i + 2$, i and $i + 3$, i and $i + 4$, and i and $i + 5$. [d] As it results from the Ramachandran plot analysis. [e] As it results from the AQUA analysis excluding the nonassigned residues (*47*).

holoproteins, mobility on time scales shorter than nanoseconds was restricted to the protein termini and/or the C-terminal extra residues of the factor Xa cleavage site.

DISCUSSION

Structural Features of HAH1 in the Apo and Holo Forms. HAH1 in solution adopts the classical $\beta\alpha\beta\beta\alpha\beta$ ferredoxin fold regardless of the presence of the metal ion. Chemical shift variations observed between apo-HAH1 and copper(I)−HAH1 (Figure 1) indicate that perturbations of the backbone structure due to copper(I) binding affect mainly the Cys-containing loop (loop 1) and the N-terminal region of the first α-helix. For the two copper(I)-binding cysteines, the largest conformational rearrangement is observed for Cys12, while the rearrangement for Cys15 is small. Secondary structure elements are maintained in both protein forms, with at most a one-residue variation in the length of β-strands β_2 and β_4 (Table 3). The behavior observed here for human HAH1 is quite different from what was reported for the yeast homologue, Atx1, where helix α_1 experiences a significant variation in length in passing from the apo to the holo form, the latter being three residues longer at the N-terminal side (*42*).

The structure of HAH1 has been determined in the solid state for the holo form loaded with various metals (copper(I), mercury(II), cadmium(II)) (*21*). The structure of the yeast homologue of HAH1, Atx1, is also available both in the oxidized apo form (*40*), where the two cysteines form a disulfide bridge, and in the mercury(II)-loaded form (*40*). In mercury(II)−HAH1 one metal ion is bound by two protein molecules, while Hg^{2+}−Atx1 is a monomer. Similarly to what was observed with mercury(II), also in the crystal structures of copper(I)−HAH1 and cadmium(II)−HAH1 the metal ion is bound by the cysteines of two protein molecules. The structures of HAH1 loaded with different metals are all very similar to one another, with maximum RMSD values between monomer pairs of 0.6 Å (*21*).

In the present work, an RMSD between the two average structures of apo-HAH1 and copper(I)−HAH1 lower than 1.0 Å is observed. The RMSDs of both average solution structures from each of the monomers of the crystal structure of copper(I)−HAH1 are between 0.9 and 1.0 Å, depending on the specific pair considered (Figure 2C,D). There are thus no major conformational rearrangements between the solid-state structures and the monomeric solution structures, also regardless of the presence of the metal ion. In agreement with the above observations, the same secondary structure elements are observed in the solid-state and solution structures. The backbone RMSD between the solution structures of copper(I)−HAH1 and copper(I)−Atx1 is ca. 1.5 Å (measured on the superposition of the backbone atoms of all corresponding residues in the two proteins). Most of the variation between the two structures is located in the loop regions, and particularly in the copper(I)-binding loop (Figure 4). A main determinant of this difference is presumably the different coordinations of the metal ion: bicoordinate in HAH1, tricoordinate in Atx1 (*29*). This appears to be associated with a longer α_1 helix, as can be observed from Figure 4. The different helix length then constrains the relative positioning of the metal-binding cysteines, and thus

Table 2: Statistical Analysis of the Energy-Minimized Family of Conformers and the Mean Structure of Cu(I)−HAH1

	REM[a] (30 structures)	⟨REM⟩[a] (mean)
RMS violations per meaningful distance constraint (Å)[b]		
intraresidue (237)	0.0225 ± 0.0359	0.0167
sequential (321)	0.0075 ± 0.0016	0.0084
medium-range (289)[c]	0.0105 ± 0.0017	0.0097
long-range (433)	0.0085 ± 0.0015	0.0070
total (1280)	0.0133 ± 0.0148	0.0103
RMS violations per meaningful dihedral angle constraints (deg)[b]		
ϕ (49)	1.6 ± 1.05	0.86
ψ (49)	0.80 ± 0.6	1.90
average number of constraints per residue	18	
average number of violations per structure		
intraresidue	9.6 ± 2.2	9
sequential	4.8 ± 1.6	6
medium-range	7.9 ± 1.9	7
long-range	5.9 ± 1.8	4
total	28.3 ± 4.4	26
ϕ	2.8 ± 1.1	1
ψ	1.2 ± 1.0	1
average number of NOE violations larger than 0.3 Å	0.03 ± 0.0	0.00
average number of NOE violations between 0.1 and 0.3 Å	2.4 ± 1.1	3.00
structural analysis[d]		
% of residues in most favorable regions	84.9	87.9
% of residues in allowed regions	14.9	12.1
% of residues in generously allowed regions	0.2	0.0
% of residues in disallowed regions	0.0	0.0
experimental restraints analysis[e]		
% completeness of experimentally observed NOEs up to a 4 Å cutoff distance	70	65
% completeness of experimentally observed NOEs up to a 5 Å cutoff distance	49	45

[a] REM indicates the energy-minimized family of 30 structures, and ⟨REM⟩ is the energy-minimized mean structure obtained from the coordinates of the individual REM structures. [b] The number of meaningful constraints for each class is reported in parentheses. [c] Medium-range distance constraints are those between residues i and $i + 2$, i and $i + 3$, i and $i + 4$, and i and $i + 5$. [d] As it results from the Ramachandran plot analysis. [e] As it results from the AQUA analysis excluding the nonassigned residues (*47*).

Table 3: Residues Involved in Secondary Structure Elements in the Apo-HAH1 and Copper(I)−HAH1 Solution Structures

secondary structure element	apo-HAH1	copper(I)−HAH1	secondary structure element	apo-HAH1	copper(I)−HAH1
β_1	3−8	3−8	β_3	39−43	39−43
α_1	14−26	14−26	α_2	48−55	48−55
β_2	31−34	30−34	β_4	62−68	63−68

may contribute to determining the coordination preferences of the copper(I) ion. The other elements of secondary structure are instead quite similar between copper(I)−HAH1 and copper(I)−Atx1 (Figure 4). Finally, it can be noted that, despite the fact that HAH1 has a pI close to 7.0, while Atx1 has a pI of ca. 8.6, the surface electrostatic potentials in the region involved in intermolecular contacts with the partner ATPase are very similar for both proteins.

It has been highlighted that within the superfamily of copper(I)-transporting chaperones there are several instances where metal binding is associated with a repacking of the hydrophobic residues in loops 1, 3, and 5, which are behind the metal ligands (Cys12 and Cys15) (*43*). In the human Menkes protein (ATP7A), the rearrangement appears to be very limited if not absent for both the second (*16*) and the fourth (*44*) domains. The hydrophobic contacts are made by Met12, Leu38, and Phe66 (numbering as in ref *16*). The present solution structures of HAH1 permit the complementary analysis for the ATP7A partner. The above-mentioned residues correspond to Met10, Leu35, and Lys60 in the present protein. Note that the nonconservative replacement of the aromatic residue 66 in ATPases with Lys60 in copper(I)−chaperones within loop 5 is observed in all eukaryotic sequences (*13*). The conformational rearrangement of the backbone of loops 1, 3, and 5 is quite small in HAH1 (Figure 2). A larger rearrangement was instead observed in Atx1 (*42*). As far as the side chains are concerned, the only significant rearrangement is experienced by that of Lys60, which points toward the copper(I) site in the holoprotein and away from the protein core in the apo form. The charged amino group of the side chain of Lys60 is located in essentially the same position with respect to the metal site in the crystal structure (*21*) and in the present solution structure of copper(I)−HAH1. The observed rearrangement could be the result of the variation in electrostatic charge in the metal-binding loop, where the two metal-binding cysteines deprotonate to bind the monopositive copper(I) ion, with a net total charge variation of −1. The movement of Lys60 closer to the copper site can therefore contribute to the stabilization of the adduct with copper. In this respect it is also to be noted that the side chain of Thr11 moves slightly away from the metal site upon metal binding.

The protein dynamics in solution as probed by ^{15}N relaxation data are similar in the apo and the copper(I)-loaded forms of HAH1. The only detectable difference is that some conformational averaging can be detected in the metal-binding loop for copper(I)−HAH1 but not for apo-HAH1 (Figure 3). Other than this, the dynamic behavior of HAH1

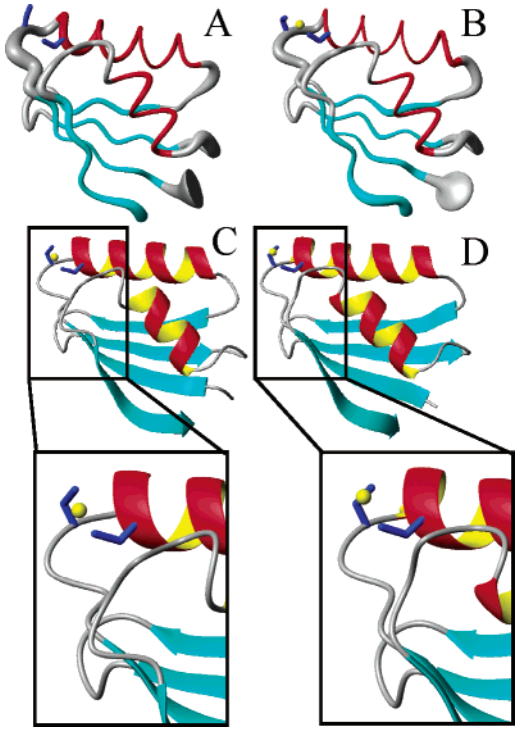

FIGURE 2: (A) Structure of apo-HAH1 compared to (B) the structure of copper(I)−HAH1. The structures are shown as a tube with variable radius, proportional to the local backbone RMSD. Regions of regular secondary structure are colored (red, α-helices; cyan, *β*-sheets). In the structure of copper(I)−HAH1 the copper ion is shown as a yellow sphere, and the side chains of the coordinating Cys are shown as blue sticks. (C) The energy-minimized average solution structure is compared with (D) the first molecule in the dimeric X-ray structure of copper(I)−HAH1. Both structures are shown as ribbons, and the copper site is shown as in (A) and (B). The two insets show an expansion of the copper(I) site and its surroundings in the solution and X-ray structures. This figure was prepared with MOLMOL (*48*).

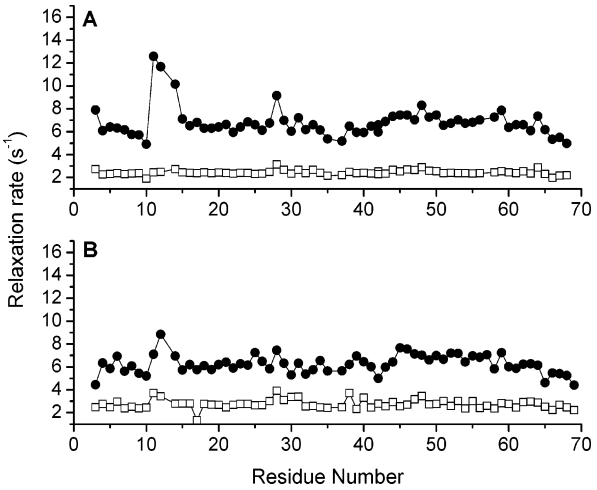

FIGURE 3: ^{15}N R_1 (open squares) and R_2 (filled circles) relaxation rates for (A) copper(I)−HAH1 and (B) apo-HAH1.

appears relatively uniform throughout the protein sequence, in both protein forms. Instead, in yeast Atx1 there is more conformational averaging present in the apoprotein than in the copper(I)-loaded protein (*20*). These differences are not located in the metal-binding site but rather in the regions adjacent to it (particularly loop 5 and the C-terminal part of helix α_2). Overall, there are more residues experiencing

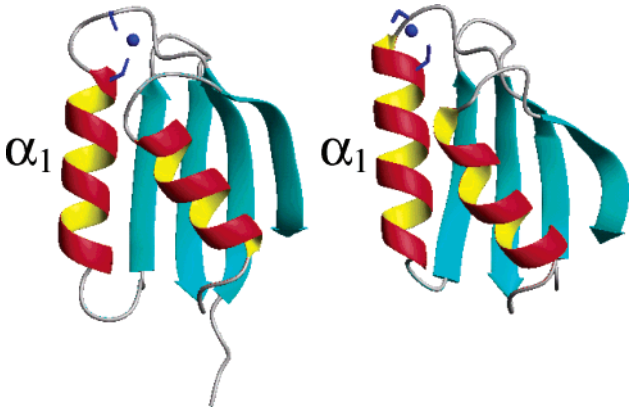

FIGURE 4: Comparison of the average solution structures of copper(I)−HAH1 (right) and copper(I)−Atx1 (left, PDB entry 1FD8 (*42*)). The side chains of the copper(I)-binding cysteines and the metal ion are shown. Helix α_1 is labeled. This figure was prepared with MOLMOL (*48*).

metalation-dependent variations in their dynamic properties in Atx1 than in HAH1.

Aggregation State of HAH1 and Metal Coordination. There are many reports in the literature that copper chaperones may form dimers in the apo and/or copper(I)-loaded forms, depending on the experimental conditions. For HAH1, this is clearly shown by the fact that the protein forms a copper(I)-bridged dimer in the crystal structure (*21*), while it is monomeric in the present solution structure. EXAFS (*41*) and isothermal calorimetry (ITC) (*18*) measurements indicate that in solution HAH1 binds one single copper ion per protein molecule with an affinity constant around 2×10^5 M^{-1}. EXAFS data clearly demonstrated that there is a dependence of the coordination environment of copper(I) in HAH1 on the presence of exogenous thiols and on the procedure used for metalation (*41*). Analogous conclusions have been reached for homologous bacterial proteins, such as *Bacillus subtilis* CopZ (*45*) or *Enterococcus hirae* CopZ (*46*), but not for yeast Atx1 (*42*). The relative role and importance of phenomena such as aspecific aggregation, protein dimerization, and coordination of small reductant/buffer molecules is strongly dependent on the system and the experimental conditions used.

It seems that copper tends to recruit ligands in addition to the two provided by one protein molecule. It therefore can additionally bind to suitable buffer or reductant molecules, or can bind another cysteine side chain from a second protein molecule. Furthermore, more complex species can form involving dicopper clusters where two holoprotein molecules form adducts through one or two buffer or reductant molecules and bridge the two copper(I) ions (*45*). Some of these configurations can be "locked" through crystallization and consequently be detected in X-ray diffraction experiments as shown for copper(I)−HAH1 (*21*). However, the absolute energy difference between the various species is probably small, so that in solution one or the other can become dominant depending on the fine details of sample conditions and composition.

All of the above observations are instrumental to protein function. Indeed, copper(I) transfer from the chaperone to the partner ATPase is most likely to happen by way of an intermediate state with a single copper(I) ion bridging the two partners (*19*). The small, environment-sensitive differ-

ence in energy between monomers and homodimers suggests that the above intermediate state forms with a quite low energy loss, thereby permitting rapid transfer. The sensitivity to the environment could also be useful in modulating the kinetics of the transfer reaction as a function of physiological conditions. It is also to be noted that the significant electrostatic charge that is present at the surface of eukaryotic copper chaperones should be detrimental for the formation of homodimers, which is thus mainly the result of copper(I) coordination chemistry. This aspect is clearly quite different when heterodimers between the chaperone and the ATPase are involved.

CONCLUDING REMARKS

The structure and dynamics of human HAH1 in solution have been characterized by heteronuclear NMR methods. As expected, HAH1 adopts the ferredoxin fold regardless of its metalation state. The present solution structure of monomeric copper(I)−HAH1 is different from the crystal structure of the same protein, where two protein molecules were found to coordinate a single metal ion although the protein fold is the same. Conformational rearrangements upon copper(I) binding are small, the most prominent feature being a movement of the side chain of Lys60 toward the metal site.

Some meaningful differences with respect to yeast Atx1 have been detected. The largest structural difference is related to the different coordinations of copper(I) in the two systems, which are apparently accompanied by a variation in the length of helix α_1. In general, metal-dependent structural and dynamic differences appear larger in Atx1 than in HAH1.

In conclusion, the present work provides a detailed characterization of HAH1 in both its physiologically relevant metalation states, which was lacking. The subtle differences observed with respect to Atx1 may indicate the limits where the yeast and human systems, though homologous, start differentiating from the biochemical point of view. Indeed, metal homeostasis processes must be different for monocellular and pluricellular organisms, as indeed proved by the different sequence lengths and numbers of metal-binding domains of their ATPases.

ACKNOWLEDGMENT

We acknowledge the "Centro Interdipartimentale di Spettroscopia di Massa" for mass spectroscopy measurements. We thank Prof. R. Udisti for atomic absorption measurements and Prof. A. Quattrone for providing us with cDNA. Ms. Maria Katsarou is thanked for her help in the protein preparation.

SUPPORTING INFORMATION AVAILABLE

Six tables showing the experiments performed, the chemical shift assignments, and the upper distance limits used in structure calculations for apo-HAH1 and copper(I)−HAH1. This material is available free of charge via the Internet at http://pubs.acs.org.

REFERENCES

1. Linder, M. C. (1991) *Biochemistry of Copper*, Plenum Press, New York.
2. Vulpe, C. D., and Packman, S. (1995) Cellular copper transport, *Annu. Rev. Nutr. 15*, 293−322.
3. O'Halloran, T. V., and Culotta, V. C. (2000) Metallochaperones: An Intracellular Shuttle Service for Metal Ions, *J. Biol. Chem. 275*, 25057−25060.
4. Harrison, M.D., Jones, C. E., Solioz, M., and Dameron, C. T. (2000) Intracellular copper routing: the role of copper chaperones, *Trends Biochem. Sci. 25* (1), 29−32.
5. Puig, S., and Thiele, D. J. (2002) Molecular mechanisms of copper uptake and distribution, *Curr. Opin. Chem. Biol. 6* (2), 171−180.
6. Huffman, D. L., and O'Halloran, T. V. (2000) Energetics of Copper Trafficking Between the Atx1 Metallochaperone and the Intracellular Copper-transporter, Ccc2, *J. Biol. Chem. 275*, 18611−18614.
7. Rae, T., Schmidt, P. J., Pufahl, R. A, Culotta, V. C., and O'Halloran. T. V. (1999) Undetectable intracellular free copper: the requirement of a copper chaperone for superoxide dismutase, *Science 284*, 805−808.
8. Rosenzweig, A. C. (2001) Copper delivery by metallochaperone proteins, *Acc. Chem. Res. 34* (2), 119−128.
9. Banci, L., and Rosato, A. (2003) Structural genomics of proteins involved in copper homeostasis, *Acc. Chem. Res. 36*, 215−221.
10. Klomp, L. W., Lin, S. J., Yuan, D., Klausner, R. D., Culotta, V. C, and Gitlin, J. D. (1997) Identification and functional expression of HAH1, a novel human gene involved in copper homeostasis, *J. Biol. Chem. 272*, 9221−9226.
11. Pufahl, R. A., Singer, C. P., Peariso, K. L., et al. (1997) Metal ion chaperone function of the soluble Cu(I) receptor Atx1, *Science 278*, 853−856.
12. Petris, M. J., Mercer, J. F., Culvenor, J. G., Lockhart, P., and Camakaris, J. (1996) Ligand-regulated transport of the Menkes copper P-type ATPase efflux pump from the Golgi apparatus to the plasma membrane: a novel mechanism of regulated trafficking, *EMBO J. 15*, 6084−6095.
13. Arnesano, F., Banci, L., and Bertini, I., et al. (2002) Metallochaperones and metal transporting ATPases: a comparative analysis of sequences and structures, *Genome Res. 12*, 255−271.
14. Walker, J. M., Huster, D., Ralle, M., Morgan, C. T., Blackburn, N. J., and Lutsenko, S. (2004) The N-terminal metal-binding site 2 of the Wilson's disease protein plays a key role in the transfer of copper from Atox1, *J. Biol. Chem. 279*, 15376−15384.
15. Jones, C. E., Daly, N. L., Cobine, P. A., Craik, D. J., and Dameron, C. T. (2003) Structure and metal binding studies of the second copper binding domain of the Menkes ATPase, *J. Struct. Biol. 143* (3), 209−218.
16. Banci, L., Bertini, I., Del Conte, R., D'Onofrio, M., Rosato, A. (2004) Solution structure and backbone dynamics of the Cu(I) and apo-forms of the second metal-binding domain of the Menkes protein ATP7A, *Biochemistry 43*, 3396−3403.
17. Strausak, D., Howie, M. K., Firth, S. D., et al. (2003) Kinetic analysis of the interaction of the copper chaperone Atox1 with the metal binding sites of the Menkes protein, *J. Biol. Chem. 278* (23), 20821−20827.
18. Wernimont, A. K., Yatsunyk, L. A., and Rosenzweig, A. C. (2004) Binding of copper(I) by the Wilson disease protein and its copper chaperone, *J. Biol. Chem. 279* (13), 12269−12276.
19. Arnesano, F., Banci, L., Bertini, I., and Bonvin, A. M. J. J. (2004) A docking approach to the study of copper trafficking proteins: interaction between metallochaperones and soluble domains of copper ATPases, *Structure 12*, 669−676.
20. Arnesano, F., Banci, L., and Bertini, I., et al. (2001) Characterization of the binding interface between the copper chaperone Atx1 and the first cytosolic domain of Ccc2 ATPase, *J. Biol. Chem. 276* (44), 41365−41376.
21. Wernimont, A. K., Huffman, D. L., Lamb, A. L., O'Halloran, T. V., and Rosenzweig, A. C. (2000) Structural basis for copper transfer by the metallochaperone for the Menkes/Wilson disease proteins, *Nat. Struct. Biol. 7* (9), 766−771.
22. Eccles, C., Güntert, P., Billeter, M., and Wüthrich, K. (1991) Efficient analysis of protein 2D NMR spectra using the software package EASY, *J. Biomol. NMR 1*, 111−130.
23. Güntert, P., Braun, W., and Wüthrich, K. (1991) Efficient computation of three-dimensional protein structures in solution from Nuclear Magnetic Resonance data using the program DIANA and the supporting programs CALIBA, HABAS and GLOMSA, *J. Mol. Biol. 217*, 517−530.
24. Vuister, G. W., and Bax, A. (1993) Quantitative J Correlation: A New Approach for Measuring Homonuclear Three-Bond $J(H^NH^\alpha)$ Coupling Constants in ^{15}N Enriched Proteins, *J. Am. Chem. Soc. 115*, 7772−7777.

25. Gagne', R. R, Tsuda, S, Li, M. X., Chandra, M., Smillie, L. B, and Sykes, B. D. (1994) Quantification of the calcium-induced secondary structural changes in the regulatory domain of troponin-C, *Protein Sci. 3*, 1961−1974.
26. Wishart, D. S., and Sykes, B. D. (1994) The ^{13}C chemical shift index: a simple method for the identification of protein secondary structure using ^{13}C chemical shift data, *J. Biomol. NMR 4*, 171−180.
27. Güntert, P., Mumenthaler, C., and Wüthrich, K. (1997) Torsion Angle Dynamics for NMR Structure Calculation with the new program DYANA, *J. Mol. Biol. 273*, 283−298.
28. Herrmann, T., Güntert, P., and Wüthrich, K. (2002) Protein NMR structure determination with automated NOE assignment using the new software CANDID and the torsion angle dynamics algorithm DYANA, *J. Mol. Biol. 319* (1), 209−227.
29. Banci, L., Bertini, I., Ciofi-Baffoni, S., Huffman, D. L., and O'Halloran, T. V. (2001) Solution structure of the yeast copper transporter domain Ccc2a in the apo and Cu(I)-loaded states, *J. Biol. Chem. 276* (11), 8415−8426.
30. Case, D. A., Pearlman, D. A., Caldwell, J. W., et al. (1999) AMBER 6, University of California, San Francisco.
31. Banci, L., Benedetto, M., Bertini, I., Del Conte, R., Piccioli, M., and Viezzoli, M. S. (1998) Solution structure of reduced monomeric Q133M2 Copper, Zinc Superoxide Dismutase. Why is SOD a dimeric enzyme? *Biochemistry 37*, 11780−11791.
32. Laskowski, R. A., MacArthur, M. W., Moss, D. S., and Thornton, J. M. (1993) PROCHECK: a program to check the stereochemical quality of protein structures, *J. Appl. Crystallogr. 26*, 283−291.
33. Laskowski, R. A., Rullmann, J. A. C., MacArthur, M. W., Kaptein, R., and Thornton, J. M. (1996) AQUA and PROCHECK-NMR: Programs for checking the quality of protein structures solved by NMR, *J. Biomol. NMR 8*, 477−486.
34. Kay, L. E., Nicholson, L. K., Delaglio, F., Bax, A., and Torchia, D. A. (1992) Pulse sequences for removal of the effects of cross correlation between dipolar and chemical-shift anisotropy relaxation mechanisms on the measurement of heteronuclear T_1 and T_2 values in proteins, *J. Magn. Reson. 97*, 359−375.
35. Grzesiek, S., and Bax, A. (1993) The importance of not saturating H2O in protein NMR. Application to sensitivity enhancement and NOE measurements, *J. Am. Chem. Soc. 115*, 12593−12594.
36. Marquardt, D. W. (1963) An algorithm for least-squares estimation of nonlinear parameters, *J. Soc. Ind. Appl. Math. 11*, 431−441.
37. Mandel, M. A., Akke, M., and Palmer, A. G., III (1995) Backbone dynamics of *Escherichia coli* ribonuclease HI: correlations with structure and function in an active enzyme, *J. Mol. Biol. 246*, 144−163.
38. Cavanagh, J., Fairbrother, W. J., Palmer, A. G., III, and Skelton, N. J. (1996) *Protein NMR Spectroscopy. Principles and practice*, Academic Press, San Diego.
39. Grzesiek, S., Bax, A., and Clore, G. M., et al. (1996) The solution structure of HIV-1 Nef reveals an unexpected fold and permits delineation of the binding surface for the SH3 domain of Hck tyrosine protein kinase, *Nat. Struct. Biol. 3* (4), 340−345.
40. Rosenzweig, A. C., Huffman, D. L., Hou, M. Y., Wernimont, A. K., Pufahl, R. A., and O'Halloran, T. V. (1999) Crystal structure of the Atx1 metallochaperone protein at 1.02 A resolution, *Struct. Fold Des. 7*, 605−617.
41. Ralle, M., Lutsenko, S., and Blackburn, N. J. (2003) X-ray absorption spectroscopy of the copper chaperone HAH1 reveals a linear two-coordinate Cu(I) center capable of adduct formation with exogenous thiols and phosphines, *J. Biol. Chem. 278* (25), 23163−23170.
42. Arnesano, F., Banci, L., Bertini, I., Huffman, D. L., and O'Halloran, T. V. (2001) Solution Structure of the Cu(I) and Apo forms of the Yeast Metallochaperone, Atx1, *Biochemistry 40* (6), 1528−1539.
43. Banci, L., Bertini, I., and Del Conte, R. (2003) The solution structure of apo CopZ from *Bacillus subtilis*: a further analysis of the changes associated with the presence of copper, *Biochemistry 42* (46), 13422−13428.
44. Gitschier, J., Moffat, B., Reilly, D., Wood, W. I., and Fairbrother, W. J. (1998) Solution structure of the fourth metal-binding domain from the Menkes copper-transporting ATPase, *Nat. Struct. Biol. 5*, 47−54.
45. Banci, L., Bertini, I., Del Conte, R., Mangani, S., and Meyer-Klaucke, W. (2003) X-ray absorption spectroscopy study of CopZ, a copper chaperone in *Bacillus subtilis.* The coordination properties of the copper ion, *Biochemistry 8*, 2467−2474.
46. Urvoas, A., Moutiez, M., Estienne, C., Couprie, J., Mintz, E., and Le Clainche, L. (2004) Metal-binding stoichiometry and selectivity of the copper chaperone CopZ from Enterococcus hirae, *Eur. J. Biochem. 271* (5), 993−1003.
47. Laskowski, R. A., MacArthur, M. W., and Thornton, J. M. (1998) Validation of protein models derived from experiment, *Curr. Opin. Struct. Biol. 8*, 631−639.
48. Koradi, R., Billeter, M., and Wüthrich, K. (1996) MOLMOL: a program for display and analysis of macromolecular structure, *J. Mol. Graphics 14*, 51−55.

BI0487591